Composite Structures 94 (2012) 3194–3206

Contents lists available at SciVerse ScienceDirect

Composite Structures

journal homepage: www.elsevier.com/locate/compstruct

In-plane and out-of-plane dynamics and buckling of functionally graded circular curved beams

M.T. Piovan [a,*], S. Domini [a,b], J.M. Ramirez [a]

[a] Centro de Investigaciones en Mecánica Teórica y Aplicada, Universidad Tecnológica Nacional-F.R.B.B., 11 de Abril 461, Bahía Blanca, BA B8000LMI, Argentina
[b] Departamento de Ingeniería Electrica, Universidad Tecnologica Nacional-F.R.B.B., 11 de Abril 461, Bahía Blanca, BA B8000LMI, Argentina

ARTICLE INFO

Article history:
Available online 22 May 2012

Keywords:
Functionally graded materials
Curved beams
Dynamics
Buckling
Initial stresses
Shear deformability

ABSTRACT

In this paper the dynamic and buckling features of slender structures with curved axis are addressed. A survey on the literature concerning mechanics of beams constructed with non-homogeneous materials or with functionally graded materials reveals only a few papers devoted to the dynamics and buckling of curved beams constructed with such materials. This problem was tackled mainly through 2D or 3D numerical formulations, but comprehensive beam theories on the matter are scarce. In the present paper a model of non-homogeneous and/or FGM curved beams is developed. The model is deduced by adopting a consistent displacement field which incorporates second order rotational terms based on the semi-tangential rule. The model also incorporates the shear flexibility due to bending and warping due to twisting effects. Arbitrary initial stresses and initial off-axis loads are taken into account in the linearized principle of virtual works. The finite element method is employed to discretize the motion equations with the objective to solve problems of dynamics, statics and buckling. The model contains, as particular cases, several straight beam theories as well as curved beam theories. Some comparisons with the available experimental data of the open literature are performed in order to illustrate the predictive features of the model, and comparisons with 2D and 3D finite element approaches are also performed.

1. Introduction

Non-homogeneous materials with properties that can vary gradually along a given direction have emerged as an alluring option to solve the problem of high stress gradients (both normal and tangential) induced in specimens constructed with layers of two or more different materials (e.g. metals and ceramics). It was observed that in structures with layered configurations subjected to thermo-mechanical loads, the resultant stress gradients may reach high values such that the structure can suffer for debonding or the beginning of cracks that eventually can cause a general failure. The concept of a material with graded properties was firstly explored in the early seventies to design effective thermal barriers in turbine blades. Later, in the middle eighties the concept functionally graded materials was established to identify a particular manufacturing process developed in Japan. Thereafter there was a remarkable interest to produce these materials and employ them, especially in high technology military aircrafts, aerospace actuators, special sensors and for medical uses too. In the last ten to twelve years, many researchers focused their attention to study shells and solids constructed with FGM. In the works of Reddy [1], Reddy and Chin [2], Praveen et al. [3], Kitipornchai et al. [4], Hosseini Kordkheili and Naghdabadi [5], Cheng and Batra [6] among others, studies about non-homogeneous shells, plates and solids with graded properties can be found. Other investigations about functionally graded straight beams or straight cylinders can be followed in the works of Chakraborty et al. [7], Goupee and Vel [8], Ding et al. [9], Lu et al. [10] and Batra [11], among others. In these papers three dimensional or two dimensional models representing a beam were presented with the aim to characterize the state of stresses, strains or displacements analytically [8–11] or by means of finite element approaches [7]. In some papers hypotheses of plane stresses [7–10] or plane strains [8] were employed to construct the model. The solution of the pure torsion problem of a functionally graded bar was tackled by Batra [11]. In all previous works, in addition to developing new models, several ways to define the distribution of the graded material properties were introduced. The distribution of material properties along given directions plays an important role in the structural response. The most common way to define a graded material property is by means of power laws in the cross-section. Exponential forms are also used. This last type allows the simplification of mathematical forms in order to reach to closed form solutions. Other graded distributions are sought for particular structural responses or to optimize static or dynamic responses [8].

* Corresponding author. Tel.: +54291 4555220; fax: +54291 4555311.
E-mail address: mpiovan@frbb.utn.edu.ar (M.T. Piovan).

0263-8223/$ - see front matter © 2012 Elsevier Ltd. All rights reserved.
http://dx.doi.org/10.1016/j.compstruct.2012.04.032

Although in the international scientific literature, there is a lot of research on the mechanics of straight beams constructed with FGM, it should be noted that the investigations on the mechanics of curved beams with functionally graded properties are scarce. Dryden [12] and Malekzadeh [13] among others developed curved beam model appealing to 2D formulations. Actually, Dryden [12] carried out a study on a curved beam by means of an approximation to a 2D description based on the hypothesis of plane stresses. Malekzadeh [13] carried out studies for in-plane vibrations of arches in the context of 2D formulations. Malekzadeh et al. [14] introduced a model for out-of-plane vibrations of curved beams made of FGM considering thermal effects. Piovan et al. [15] deduced a one dimensional model of curved beams appealing to the variational principle of Hellinger–Reissner. Yousefi and Rastgoo [16] developed a one dimensional model for free vibrations of spatial curved beams constructed with graded materials. Filipich and Piovan [17] deduced a theory of thick arches employing a classical strength of material approach. However these last two models were restricted to in-plane motions. Apparently Shafiee et al. [18] were the firsts in developing a theory incorporating in-plane and out-of-plane motions in a curved beam with graded material properties; however this model was employed to calculate only buckling loads, moreover shear flexibility was not incorporated and dynamic problems were not considered. It should be remarked that there is a scarce information related to dynamic analysis of functionally graded curved beams subjected to arbitrary initial stresses and off-axis initial loads.

The aim of the present paper is focused on developing a one dimensional model of curved beams with graded properties. The model is conceived in order to incorporate, in a unified fashion, the in-plane motion and the out-of-plane motion together with their coupling due to the constitutive effects as well as mechanical and thermo-elastic effects. To avoid misunderstandings in this paper, in-plane motion and out-of-plane motion imply the movement in the plane of the beam curvature (the case usually analyzed in 2D theories) and the movement normal to that plane, respectively. The shear flexibility due to bending and twisting is taken into account. The effect of warping due to non-uniform torsion is also considered. It has to be mentioned that very few papers of the open literature incorporate warping and twisting neither in the context of functionally graded or non-homogeneous curved beams nor in straight beams. It is known that these topics are important for certain types of cross-sections and crucial for example in the case of open thin walled beams. The model is developed by adopting a displacement field which contains linear and second order terms related to rotational kinematic variables. The linearized principle of virtual works [19–21] is employed in order to obtain the motion equations. The resulting model consists of a set of seven differential equations elastically coupled. However depending on the type of gradation law involved and the features of the cross-section the full system can be decoupled into two subsystems, i.e. one system representing in-plane motions and the other representing out-of-plane motions. The model is discretized with an isoparametric finite element. Problems of statics, free vibrations with or without the presence of initial stresses are analyzed. Comparisons with the available experimental data are also performed.

2. Model development

2.1. Hypotheses and kinematic relations

In Fig. 1 a sketch of the curved beam is shown. The main reference system {**C**: *xyz*} is located at the geometric center of the cross-section, where the *x*-axis is tangent to the circular axis of the beam, whereas *y* and *z* are axes belonging to the cross-section, but not necessarily the principal ones. In the aforementioned figure two details are shown with the possible cross-sectional configurations: a solid shape and a thin-walled shape. Another reference system {**A**: xx_cx_w} has to be employed as a secondary reference in the case of thin walled beams. This reference system is located in the middle line of the cross-sectional wall and it is used to describe the constitutive equations. The curved axis of the beam, with constant radius R, is contained in the plane Ξ. The curved beam has an opening angle β and a length $L = R\beta$. The present curved beam theory is based on the following assumptions:

1 The cross-section contour is rigid in its own plane.
2 The warping function is defined with respect to point **C**.
3 Material properties can vary with an arbitrary function within the cross-section.
4 The stress tensor, the volume forces and surface forces are composed by initial and incremental terms.
5 The displacement field is described with first and second order rotational parameters that are defined according to the rule of semi-tangential rotations.
6 Inertial effects due to higher order displacements are neglected.
7 Structural damping is included within the context of the finite element method through a proportional Rayleigh model.
8 Hypotheses of transverse isotropy are considered for the graded materials.

Taking into account Assumptions 1, 2 and 5 it is possible to construct [20,21] the displacement field of an arbitrary point in the curved beam (including first-order and second-order terms of rotation parameters). Then the linear and non-linear components of the displacement field can be written in the following form [20]:

$$\begin{Bmatrix} u_x^L \\ u_y^L \\ u_z^L \end{Bmatrix} = \begin{Bmatrix} u_{xc} - \omega\Phi_W \\ u_{yc} \\ u_{zc} \end{Bmatrix} + \begin{bmatrix} 0 & -\Phi_3 & \Phi_2 \\ \Phi_3 & 0 & -\Phi_1 \\ -\Phi_2 & \Phi_1 & 0 \end{bmatrix} \begin{Bmatrix} 0 \\ y \\ z \end{Bmatrix}, \tag{1}$$

$$\begin{Bmatrix} u_x^{NL} \\ u_y^{NL} \\ u_z^{NL} \end{Bmatrix} = \frac{1}{2} \begin{bmatrix} -\Phi_3^2 - \Phi_2^2 & \Phi_1\Phi_2 & \Phi_1\Phi_3 \\ \Phi_1\Phi_2 & -\Phi_1^2 - \Phi_3^2 & \Phi_2\Phi_3 \\ \Phi_1\Phi_3 & \Phi_2\Phi_3 & -\Phi_1^2 - \Phi_2^2 \end{bmatrix} \begin{Bmatrix} 0 \\ y \\ z \end{Bmatrix}, \tag{2}$$

where, u_{xc}, u_{yc}, u_{zc} are the displacements of the reference point **C**; ϕ_x is the twisting parameter; θ_y and θ_z are bending rotational parameters, and finally θ_x is a parameter that gives the warping intensity. ω is the warping function of the curved beam, Φ_W, Φ_1, Φ_2 and Φ_3 are defined in terms of rotational and warping parameters as follows:

$$\Phi_1 = \phi_x, \quad \Phi_2 = \theta_y, \quad \Phi_3 = \theta_z - \frac{u_{xc}}{R}, \quad \Phi_W = \theta_x + \frac{\theta_y}{R} \tag{3}$$

The warping function of the cross-section of a curved beam can be approximated [22] in the following form:

$$\omega = \bar{\omega}\mathcal{F}, \quad with \quad \mathcal{F} = \frac{R}{R+y}, \tag{4}$$

where, $\bar{\omega}$ is the warping function deduced from the Saint Venant problem of pure torsion of a straight beam. In the Appendix A a scheme to calculate the function $\bar{\omega}$ is presented.

2.2. Principle of virtual works

According to Assumptions 3–6, it is possible to define a linearized expression of the principle of the virtual works of a body subjected to a state of arbitrary initial stresses [19]. Then, defining σ_{ij} and σ_{ij}^0 as the incremental and initial stresses; $\overline{X}_i$ and $\overline{X}_i^0$ as the incremental and initial volume forces applied in the domain V; $\overline{S}_i$

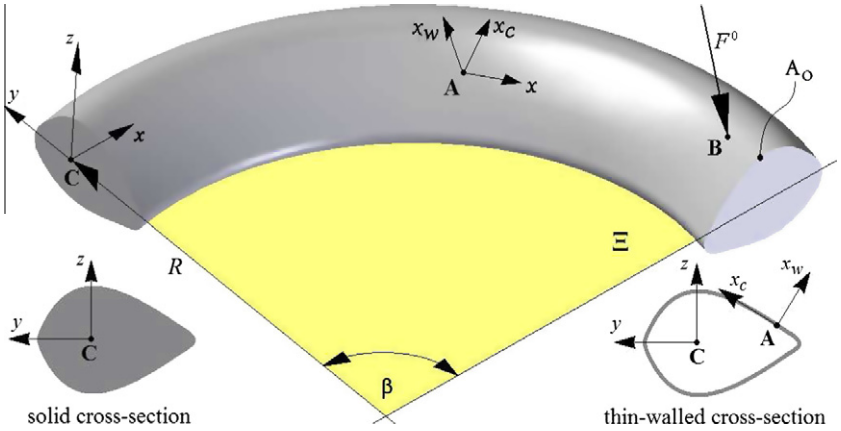

Fig. 1. Structural model: curved beam with general cross-section.

and $\overline{S}_i^0$ as the incremental and initial surface forces applied in the domain S; and defining the density with $\rho = \rho(y,z)$, then the linearized principle of virtual works can be written in the following form [19]:

$$\mathcal{W}_T = \int_V \sigma_{ij}\delta\varepsilon_{ij}^L dV + \int_V \sigma_{ij}^0\delta\varepsilon_{ij}^{NL} dV - \int_S \overline{S}_i^0\delta u_i^{NL} dS - \int_V \overline{X}_i^0\delta u_i^{NL} dV - \int_V \overline{X}_i\delta u_i^L dV - \int_S \overline{S}_i\delta u_i^L dS + \int_V \rho\ddot{u}_i^L\delta u_i^L dV = 0, \tag{5}$$

$$\mathcal{W}_T^0 = \int_V \sigma_{ij}^0\delta\varepsilon_{ij}^L dV - \int_V \overline{X}_i^0\delta u_i^L dV - \int_S \overline{S}_i^0\delta u_i^L dS = 0, \tag{6}$$

Eq. (5) is subjected to the constraint Eq. (6), which implies the condition of self-equilibrium of initial stresses and initial volume and surface forces. The first term of Eq. (5) is the virtual work due to internal forces, the second term is the virtual work due to initial stresses, the third and fourth terms are the virtual work of initial volume and surface forces due to non-linear components of displacement field, the fifth and sixth terms are the virtual work of incremental volume and surface forces due to linear components of displacement field. The seventh term of Eq. (5) is the virtual work of inertial forces, where $\ddot{u}_i^L$ are the acceleration components of a point. Dots over the variables will be interpreted as derivation with respect to the time. ε_{ij}^L are the typical linear strain tensor components, whereas ε_{ij}^{NL} are non-linear strains components, given by the following expressions:

$$\varepsilon_{ij}^L = \frac{1}{2}\left(\frac{\partial u_j^L}{\partial x_i} + \frac{\partial u_i^L}{\partial x_j}\right), \quad \varepsilon_{ij}^{NL} \cong \frac{1}{2}\left(\frac{\partial u_j^{NL}}{\partial x_i} + \frac{\partial u_i^{NL}}{\partial x_j}\right) + \frac{1}{2}\left(\frac{\partial u_h^L}{\partial x_i}\frac{\partial u_h^L}{\partial x_j}\right). \tag{7}$$

The higher-order strain tensor components due to second-order displacements are neglected in the Green–Lagrange strain tensor [20,21]. The extended forms of the strain tensor components in Eq. (7) can be found in the open literature related to curved beams [19–22].

Now, substituting Eqs. (1), (2) into Eq. (7) and then into Eq. (5) the following expression of the principle of virtual works is obtained:

$$\mathcal{W}_T = \int_L \left(\delta\widetilde{\mathbf{D}}_N^T\widetilde{\mathbf{Q}}_N + \delta\widetilde{\mathbf{D}}_C^T\widetilde{\mathbf{Q}}_C\right)dx + \int_L \delta\widetilde{\mathbf{U}}^T\mathbf{M}_m\ddot{\widetilde{\mathbf{U}}}dx - \int_L \delta\widetilde{\mathbf{U}}^T\widetilde{\mathbf{P}}_X dx \int_L \delta\widetilde{\mathbf{D}}_G^T\mathbf{T}^0\widetilde{\mathbf{D}}_G dx - \int_L \delta\widetilde{\mathbf{U}}^T\mathbf{C}_X^0\widetilde{\mathbf{U}}dx - \delta\widetilde{\mathbf{U}}^T\mathbf{C}_S^0\widetilde{\mathbf{U}} = 0 \tag{8}$$

where the displacement vector $\widetilde{\mathbf{U}}$, the deformation vectors $\widetilde{\mathbf{D}}_N$, $\widetilde{\mathbf{D}}_C$, $\widetilde{\mathbf{D}}_G$, the internal force vectors $\widetilde{\mathbf{Q}}_N$, $\widetilde{\mathbf{Q}}_C$ are defined as follows:

$$\begin{aligned}
&\widetilde{\mathbf{U}}^T = \{u_{xc}, u_{yc}, \theta_z, u_{zc}, \theta_y, \phi_x, \theta_x\}, \quad \widetilde{\mathbf{U}}_\Phi^T = \{\Phi_1, \Phi_2, \Phi_3, \Phi_w\},\\
&\widetilde{\mathbf{D}}_N^T = \{\varepsilon_{D1}, \varepsilon_{D2}, \varepsilon_{D3}, \varepsilon_{D4}\}, \quad \widetilde{\mathbf{D}}_C^T = \{\varepsilon_{D5}, \varepsilon_{D6}, \varepsilon_{D7}, \varepsilon_{D8}\},\\
&\widetilde{\mathbf{D}}_G^T = \left\{\widetilde{\mathbf{D}}_N^T, \widetilde{\mathbf{D}}_C^T, \widetilde{\mathbf{U}}_\Phi^T, \frac{\partial\widetilde{\mathbf{U}}_\Phi^T}{\partial x}\right\},\\
&\widetilde{\mathbf{Q}}_N^T = \{Q_x, M_y, M_z, B\}, \quad \widetilde{\mathbf{Q}}_C^T = \{Q_y, Q_z, T_w, T_{sv}\},
\end{aligned} \tag{9}$$

whereas for the sake of fluid and clear reading, the matrix of the initial stress resultants $\mathbf{T}^0$, the matrices of initial forces $\mathbf{C}_X^0$ and $\mathbf{C}_S^0$, the matrix of mass coefficients $\mathbf{M}_m$ and the vector $\widetilde{\mathbf{P}}_X$ of external forces are detailed in Appendix B. In Eq. (9) the following definitions are introduced:

$$\begin{aligned}
&\varepsilon_{D1} = \frac{\partial u_{xc}}{\partial x} + \frac{u_{yc}}{R}, \varepsilon_{D2} = \frac{\partial\theta_y}{\partial x} - \frac{\phi_x}{R}, \varepsilon_{D3} = \frac{\partial\theta_z}{\partial x} - \frac{1}{R}\frac{\partial u_{xc}}{\partial x}, \varepsilon_{D4} = \frac{\partial\theta_x}{\partial x} + \frac{1}{R}\frac{\partial\theta_y}{\partial x},\\
&\varepsilon_{D5} = \frac{\partial u_{yc}}{\partial x} - \theta_z, \varepsilon_{D6} = \frac{\partial u_{zc}}{\partial x} + \theta_y, \varepsilon_{D7} = \frac{\partial\phi_x}{\partial x} - \theta_x, \varepsilon_{D8} = \frac{\partial\phi_x}{\partial x} + \frac{\theta_y}{R},
\end{aligned} \tag{10}$$

$$\begin{aligned}
&\{Q_x, M_y, M_z, B\} = \int_A \sigma_{xx}\{1, z, -y, -\omega\}dydz,\\
&\{Q_y, Q_z\} = \int_A \{\sigma_{xy}, \sigma_{xz}\}dydz,\\
&T_w = \int_A \left(\sigma_{xy}\frac{\partial\bar{\omega}}{\partial y} + \sigma_{xz}\frac{\partial\bar{\omega}}{\partial z}\right)dydz,\\
&T_{sv} = \int_A \left[-\sigma_{xy}\left(z + \frac{\partial\bar{\omega}}{\partial y}\right) + \sigma_{xz}\left(y - \frac{\partial\bar{\omega}}{\partial z}\right)\right]dydz.
\end{aligned} \tag{11}$$

The entities ε_{Di}, $i = 1, \ldots, 8$ may be regarded as generalized deformations. In this context ε_{D1} is the axial deformation, ε_{D2} and ε_{D3} are bending deformations, ε_{D3} is the deformation due to non-uniform warping, ε_{D5} and ε_{D6} are the bending shear deformations, ε_{D7} is the warping shear deformation and finally ε_{D8} is the pure torsion shear deformation. The internal forces Q_x, M_y, M_z, and B correspond to the axial force, the bending moment in y-direction, the bending moment in z-direction, and the bi-moment, respectively; whereas the internal forces Q_y, Q_z, T_w, and T_{sv} correspond to the shear force in y-direction, the shear force in z-direction, the twisting moment due to warping and the twisting moment due to pure torsion, respectively.

2.3. Motion equations

Performing, in Eq. (8), the conventional steps of variational calculus, it is possible to arrive to the following system of seven differential equations:

$$
\begin{aligned}
&-\frac{\partial}{\partial x}\left[Q_x-\frac{M_z}{R}+\mathcal{G}^0_{11}\right]+\mathcal{G}^0_{10}-\widetilde{\mathbf{X}}^0_1+\widetilde{\mathcal{M}}_1-\widetilde{\mathbf{P}}_{X1}=0,\\
&-\frac{\partial}{\partial x}\left[Q_y+\mathcal{G}^0_{21}\right]+\frac{Q_x}{R}+\mathcal{G}^0_{20}+\widetilde{\mathcal{M}}_2-\widetilde{\mathbf{P}}_{X2}=0,\\
&-\frac{\partial}{\partial x}\left[M_z+\mathcal{G}^0_{31}\right]-Q_y+\mathcal{G}^0_{30}-\widetilde{\mathbf{X}}^0_3+\widetilde{\mathcal{M}}_3-\widetilde{\mathbf{P}}_{X3}=0,\\
&-\frac{\partial}{\partial x}\left[Q_z+\mathcal{G}^0_{41}\right]+\mathcal{G}^0_{40}+\widetilde{\mathcal{M}}_4-\widetilde{\mathbf{P}}_{X4}=0,\\
&-\frac{\partial}{\partial x}\left[M_y+\mathcal{G}^0_{51}+\frac{B}{R}\right]+Q_z+\frac{T_{sv}}{R}+\mathcal{G}^0_{50}-\widetilde{\mathbf{X}}^0_5+\widetilde{\mathcal{M}}_5-\widetilde{\mathbf{P}}_{X5}=0,\\
&-\frac{\partial}{\partial x}\left[T_{sv}+T_w+\mathcal{G}^0_{61}\right]-\frac{M_y}{R}+\mathcal{G}^0_{60}-\widetilde{\mathbf{X}}^0_6+\widetilde{\mathcal{M}}_6-\widetilde{\mathbf{P}}_{X6}=0,\\
&-\frac{\partial}{\partial x}\left[B+\mathcal{G}^0_{71}\right]-T_w+\mathcal{G}^0_{70}+\widetilde{\mathcal{M}}_7-\widetilde{\mathbf{P}}_{X7}=0,
\end{aligned}
\tag{12}
$$

subjected to the following boundary equations:

$$
\begin{aligned}
&-\left(\overline{Q}_x-\frac{\overline{M}_z}{R}\right)+\left(Q_x-\frac{M_z}{R}\right)+\mathcal{G}^0_{11}-\widetilde{\mathbf{S}}^0_1=0,\quad or\quad \delta u_{xc}=0,\\
&-\overline{Q}_y+Q_y+\mathcal{G}^0_{21}=0,\quad or\quad \delta u_{yc}=0,\\
&-\overline{M}_z+M_z+\mathcal{G}^0_{31}-\widetilde{\mathbf{S}}^0_3=0,\quad or\quad \delta\theta_z=0,\\
&-\overline{Q}_z+Q_z+\mathcal{G}^0_{41}=0,\quad or\quad \delta u_{zc}=0,\\
&-\left(\overline{M}_y-\frac{\overline{B}}{R}\right)+\left(M_y-\frac{B}{R}\right)+\mathcal{G}^0_{51}-\widetilde{\mathbf{S}}^0_5=0,\quad or\quad \delta\theta_y=0,\\
&-\overline{T}_{sv}+\overline{T}_w+T_{sv}+T_w+\mathcal{G}^0_{61}-\widetilde{\mathbf{S}}^0_6=0,\quad or\quad \delta\phi_x=0,\\
&-\overline{B}+B+\mathcal{G}^0_{71}=0,\quad or\quad \delta\theta_x=0
\end{aligned}
\tag{13}
$$

where: $\overline{Q}_x$, $\overline{Q}_y$, $\overline{Q}_z$, $\overline{M}_z$, $\overline{M}_y$, $\overline{T}_w$, $\overline{T}_{sv}$ and $\overline{B}$ are prescribed forces that are applied on the boundaries. $\widetilde{\mathbf{S}}^0=\mathbf{C}^0_S\widetilde{\mathbf{U}}$ is a vector of resultant initial forces of surface, $\widetilde{\mathbf{X}}^0=\mathbf{C}^0_X\widetilde{\mathbf{U}}$ is a vector of resultant initial forces of volume. The non-zero components of $\widetilde{\mathbf{S}}^0$ and $\widetilde{\mathbf{X}}^0$ are associated with the variables u_{xc}, θ_z, θ_y and ϕ_x as it is shown in Appendix B. $\widetilde{\mathcal{M}}=\mathbf{M}_m\widetilde{\mathbf{U}}$ is the vector of mass forces. $\mathcal{G}^0_{j1}$ and $\mathcal{G}^0_{j0}$, $j=1,\ldots,7$ are forces and distributed forces that collect all the initial stress resultants associated with the corresponding variational variable. The expressions of $\mathcal{G}^0_{j1}$ and $\mathcal{G}^0_{j0}$ are not provided due to their extension and because they are not employed in the following paragraphs. However, the interested readers can follow a similar deduction process of $\mathcal{G}^0_{j1}$ and $\mathcal{G}^0_{j0}$ in Refs. [20,21].

2.4. Constitutive equations in terms of strain components

The stress–strain relationships, for a functionally graded material with a general distribution in the cross-section, can be represented in the following form [14]:

$$
\begin{aligned}
&\sigma_{xx}=E_{xx}(y,z)\mathcal{F}\tilde{\mathbf{g}}^T_{xx}\widetilde{\mathbf{D}}_N && \tilde{\mathbf{g}}_{xx}=\{1,z,-y,-\omega\}^T\\
&\sigma_{xy}=G_{xy}(y,z)\mathcal{F}\tilde{\mathbf{g}}^T_{xy}\widetilde{\mathbf{D}}_C, \quad with && \tilde{\mathbf{g}}_{xy}=\left\{1,0,\tfrac{\partial\bar{\omega}}{\partial y},-z-\tfrac{\partial\bar{\omega}}{\partial y}\right\}^T\\
&\sigma_{xz}=G_{xz}(y,z)\mathcal{F}\tilde{\mathbf{g}}^T_{xz}\widetilde{\mathbf{D}}_C && \tilde{\mathbf{g}}_{xz}=\left\{0,1,\tfrac{\partial\bar{\omega}}{\partial z},y-\tfrac{\partial\bar{\omega}}{\partial z}\right\}^T
\end{aligned}
\tag{14}
$$

where, $E_{xx}(y,z)$ is the longitudinal elasticity modulus, whereas $G_{xy}(y,z)$ and $G_{xz}(y,z)$ are the transversal elasticity moduli. It should be mentioned that, $G_{xy}(y,z)$ and $G_{xz}(y,z)$ may be affected by given coefficients $(\kappa_{xy},\kappa_{xz})$ in order to enhance the characterization of shear stresses, as it is done in the classic Timoshenko beam theory [19] or in other first order shear theories [14]. In recent articles [15,17] some approaches were introduced to calculate the aforementioned coefficients for the in-plane motion of curved beams.

It should be considered that material properties are function of the temperature according to the following expression [2]:

$$
m_p=p_0(c_0T^{-1}+1+c_1T+c_2T^2+c_3T^3) \tag{15}
$$

where m_p means a generic property (Young's modulus, density, Poisson's coefficient, etc.), T is the absolute temperature (^oK) and c_i are coefficients (unique for given ceramic or metallic materials) which are evaluated in order to fit experimental data [2,3]. Thus, the properties of a functionally graded material can be represented in terms of the geometry and the temperature that is calculated assuming the hypothesis of steady state thermal condition.

Now taking into account the Eq. (14), the internal forces defined in Eq. (11) can be represented in terms of generalized strains as follows:

$$
\begin{aligned}
&\widetilde{\mathbf{Q}}_N=\mathbf{J}_N\widetilde{\mathbf{D}}_N\\
&\widetilde{\mathbf{Q}}_C=\mathbf{J}_C\widetilde{\mathbf{D}}_C
\end{aligned}
\tag{16}
$$

where

$$
\begin{aligned}
&\mathbf{J}_N=\int_A E_{xx}\tilde{\mathbf{g}}_{xx}\tilde{\mathbf{g}}^T_{xx}\mathcal{F}\,dy\,dz\\
&\mathbf{J}_C=\int_A\left[G_{xy}\tilde{\mathbf{g}}_{xy}\tilde{\mathbf{g}}^T_{xy}+G_{xz}\tilde{\mathbf{g}}_{xz}\tilde{\mathbf{g}}^T_{xz}\right]\mathcal{F}\,dy\,dz
\end{aligned}
\tag{17}
$$

The Eq. (16) allows the calculation of internal forces in terms of generalized strains. Moreover, it is possible to employ Eq. (16) to calculate the internal forces of the initial equilibrium state, if vectors $\widetilde{\mathbf{D}}_N$ and $\widetilde{\mathbf{D}}_C$ of generalized incremental deformations, are substituted by $\widetilde{\mathbf{D}}^0_N$ and $\widetilde{\mathbf{D}}^0_C$, i.e. the vectors of generalized initial deformations.

2.5. A closed-form solution for free vibration

Under certain conditions it is possible to arrive to a simple closed-form solution of Eq. (12) for a free vibration problem. Thus, in the absence of initial stresses, external forces and for a beam subjected to the following boundary conditions at the ends ($x=0, x=L$):

$$
u_{yc}=u_{zc}=\phi_x=Q_x=M_y=M_z=B=0 \tag{18}
$$

the kinematic variables can be written in as harmonic functions that fulfill Eq. (18). Then after an algebraic handling it is possible to arrive to the following frequency equation:

$$
\left|k_n^2\mathbf{M}_1\mathbf{J}\mathbf{M}_1^T-k_n\left(\mathbf{M}_1\mathbf{J}\mathbf{M}_2^T-\mathbf{M}_2\mathbf{J}\mathbf{M}_1^T\right)\mathbf{M}_0+\mathbf{M}_2\mathbf{J}\mathbf{M}_2^T-\Omega^2\mathbf{M}_m\right|=0 \tag{19}
$$

where Ω is the circular frequency (rad/s), $k_n=n\pi/L$, $n=1, 2, 3, \ldots$, and $\mathbf{M}_1$, $\mathbf{M}_2$ and $\mathbf{M}_0$ are defined as follows:

$$
\mathbf{M}_1=\begin{bmatrix}
1&0&-1/R&0&0&0&0&0\\
0&0&0&0&1&0&0&0\\
0&0&1&0&0&0&0&0\\
0&0&0&0&0&1&0&0\\
0&1&0&1/R&0&0&0&0\\
0&0&0&0&0&0&1&1\\
0&0&0&1&0&0&0&0
\end{bmatrix},
$$

$$
\mathbf{M}_2=\begin{bmatrix}
0&0&0&0&0&0&0&0\\
1/R&0&0&0&0&0&0&0\\
0&0&0&0&-1&0&0&0\\
0&0&0&0&0&0&0&0\\
0&0&0&0&0&1&0&1/R\\
0&-1/R&0&0&0&0&0&0\\
0&0&0&0&0&0&-1&0
\end{bmatrix}
\tag{20}
$$

$$
\mathbf{M}_0=Diag[-1,1,-1,1,-1,1,-1],\quad \mathbf{J}=\begin{bmatrix}\mathbf{J}_N&0\\0&\mathbf{J}_C\end{bmatrix} \tag{21}
$$

Recall that $\mathbf{M}_m$ can be found in Appendix B.

3. Finite element formulation

In order to solve general problems of static, dynamic and buckling with several boundary conditions, off-axis loading and arbitrary material gradation; iso-parametric finite elements with five nodes are employed. The vector of nodal displacements $\overline{\mathbf{U}}_e$ can be arranged in the following form:

$$\overline{\mathbf{U}}_e = \{\overline{\mathbf{U}}_e^{(1)}, \ldots, \overline{\mathbf{U}}_e^{(5)}\} \tag{22}$$

where

$$\overline{\mathbf{U}}_e^{(j)} = \{u_{xc_j}, u_{yc_j}, \theta_{z_j}, u_{zc_j}, \theta_{y_j}, \phi_{x_j}, \theta_{x_j}\}, \quad j = 1, \ldots, 5 \tag{23}$$

Now, substituting Eq. (22) into Eq. (8) and applying the conventional steps of finite element procedures, it is possible to arrive to the following general discretized equation:

$$(\mathbf{K} + \mathbf{K}_G)\overline{\mathbf{W}} + \mathbf{M}\ddot{\overline{\mathbf{W}}} = \overline{\mathbf{P}} \tag{24}$$

where $\mathbf{K}$, $\mathbf{K}_G$ and $\mathbf{M}$ are the global matrices of elastic stiffness, geometric stiffness, and mass, respectively; whereas $\overline{\mathbf{W}}$, $\ddot{\overline{\mathbf{W}}}$ and $\overline{\mathbf{P}}$ are the global vectors of nodal displacements, nodal accelerations and nodal forces, respectively.

The geometric stiffness matrix can be calculated once the initial stresses are known for a given initial load configuration. In order to calculate the initial stresses the following equation has to be solved before any other calculation:

$$\mathbf{K}\overline{\mathbf{W}}^0 = \overline{\mathbf{P}}^0, \tag{25}$$

where $\overline{\mathbf{W}}^0$ and $\overline{\mathbf{P}}^0$ are the global vector of initial nodal displacements and the global vector of all initial point, volume and surface forces, respectively. The Eq. (25) corresponds to the finite element form of the self-equilibrium condition of initial stresses, initial loads and initial volume and surface forces introduced in Eq. (6).

It is important to remark that the geometric stiffness matrix $\mathbf{K}_G$ can be described as the sum of two matrices, namely $\mathbf{K}_{G1}$ and $\mathbf{K}_{G2}$. The matrix $\mathbf{K}_{G1}$ arises from the state of initial stresses that includes the virtual work of the linear components of the Green–Lagrange strains due to the non-linear components of displacements, i.e. the second integral of Eq. (5). The matrix $\mathbf{K}_{G2}$ arises from the virtual work of the general arbitrary initial off-axis loading due to the non-linear components of displacement field, i.e. a particular case of the third and fourth integrals of Eq. (5). The incorporation of matrix $\mathbf{K}_{G2}$ in the $\mathbf{K}_G$ is crucial for the calculation of lateral buckling loads or the vibration behavior under the presence of initial stresses, among others. It has to be mentioned that a geometric stiffness matrix with initial off-axis loadings similar to $\mathbf{K}_{G2}$ was firstly introduced by Argyris [31] to deal with instability problems of beams with isotropic materials but neglecting the shear flexibility of warping due to non-uniform torsion. Kim et al. [21] extended the Argyris' ideas in the context of shear deformable curved beams made of isotropic materials and Piovan and Cortínez [20] incorporated off-axis initial loads in shear deformable composite curved beams.

Eq. (24) can be modified in order to account for "a posteriori" structural proportional Rayleigh damping given by:

$$\mathbf{C}_{RD} = \eta_1\mathbf{M} + \eta_2\mathbf{K}. \tag{26}$$

The coefficients η_1 and η_2 in Eq. (26) can be computed employing two given damping coefficients (namely, ξ_1 and ξ_2) for the first and second modes, according to the common methodology presented in the bibliography related to finite element procedures [24] and vibration analysis [25]. The matrices $\mathbf{M}$ and $\mathbf{K}$ are the global mass matrix and the global elastic stiffness matrix, respectively. This leads to:

$$(\mathbf{K} + \mathbf{K}_G)\overline{\mathbf{W}} + \mathbf{C}_{RD}\dot{\overline{\mathbf{W}}} + \mathbf{M}\ddot{\overline{\mathbf{W}}} = \overline{\mathbf{P}} \tag{27}$$

For the case of free vibration analysis, the Eq. (27) can be reduced to the following eigenvalue equation when the harmonic motion $\overline{\mathbf{W}} = \overline{\mathbf{W}}^* e^{-i\Omega t}$ is prescribed and the damping effects are neglected.

$$(\mathbf{K} + \lambda\mathbf{K}_G - \Omega^2\mathbf{M})\overline{\mathbf{W}}^* = \overline{\mathbf{O}} \tag{28}$$

where $\Omega = 2\pi f$, f is the natural frequency measured in Hertz and λ is a parameter appropriately defined, in terms of beam-stress-resultants, for the characterization of initial stresses. It is possible to see that Eq. (28) allows the computation of natural frequencies (Ω or f) of beams subjected or not (this implies $\lambda \neq 0$ or $\lambda = 0$) to arbitrary initial stresses. On the other hand, the same equation can be utilized to calculate buckling loads when the condition $f = 0$ is imposed.

4. Computational analysis

In the present section numerical tests of the procedures developed in the previous sections as well as parametric studies are performed in order to check the validity and usefulness of the curved beam model and its computational approach.

Table 1 shows the properties of different metallic (Steel SUS302 and aluminium) and ceramic (Alumina Al_2O_3 and Silicon carbide SiC) materials at laboratory temperature. Table 2 shows the thermal dependence of the material properties of ZrO_2 and $Ti6Al4V$. The hypothesis of proportionality between longitudinal modulus and transversal modulus is employed in some cases to calculate the remaining elastic properties, according to recent works of the technical literature [7,17,26].

The effective material properties of the functionally graded curved beams adopted for the numerical examples are defined according to any of the following forms. The Eqs. (29)–(31) can be employed for a rectangular cross-section whereas Eq. (32) is employed for a thin-walled open cross-section.

$$p_{fgm} = p_m + (p_c - p_m)\left|\frac{2z}{b}\right|^n, \quad or \quad p_{fgm} = p_m + (p_c - p_m)\left|\frac{2y}{h}\right|^n, \tag{29}$$

$$p_{fgm} = p_m + (p_c - p_m)\left(\frac{1}{2} + \frac{z}{b}\right)^n, \quad or$$
$$p_{fgm} = p_m + (p_c - p_m)\left(\frac{1}{2} + \frac{y}{h}\right)^n, \tag{30}$$

$$p_{fgm} = p_c e^{\left[-\Lambda_p\left(\frac{1}{2} - \frac{z}{b}\right)\right]}, \quad or \quad p_{fgm} = p_c e^{\left[-\Lambda_p\left(\frac{1}{2} - \frac{y}{h}\right)\right]}, \quad with \quad \Lambda_p = Ln\left[\frac{p_c}{p_m}\right], \tag{31}$$

$$p_{fgm} = p_m + (p_c - p_m)\left|\frac{2x_w}{b_w}\right|^n \tag{32}$$

In the previous expressions p_{fgm} identifies a generic graded property (Young's Modulus, density, etc.), whereas p_c and p_m identify the homonym property for ceramic and metallic phases, respectively. In Eq. (32), x_w is the in-thickness coordinate and b_w is the wall thickness. This last type of material distribution implies that the thin-walled beam has a ceramic surface surrounding the metallic core.

4.1. Convergence tests

The first example corresponds to a convergence test of the finite element procedures. The geometrical properties of the curved beam are $R = 1.0$ m, $L = 1.0$ m, with a rectangular cross-section of $b = 0.05$ m, $h = 0.01$ m. The material properties vary from a metallic surface (SUS302 at $z = -h/2$) to a ceramic surface (Alumina at $z = h/2$) according to the exponential law given in Eq. (31).

Table 1
Material properties for metallic and ceramic components.

Properties	Steel	Alumina	Aluminium	Silicon carbide
Longitudinal modulus of elasticity (GPa)	214	390	67	302
Transversal modulus of elasticity (GPa)	80.0	137	–	–
Poisson's coefficient	–	–	0.33	0.17
Density (kg/m^3)	7800	3200	2700	3200

Table 2
Coefficients for the temperature dependent properties of ZrO_2 and *Ti6Al4V*.

Properties	Material	m_{p_0}	c_0	c_1	c_2	c_3
E (Pa)	*Ti6Al4V*	122.7×10^9	0	-4.605×10^{-4}	0	0
	ZrO_2	132.2×10^9	0	-3.805×10^{-4}	-6.127×10^{-8}	0
ν	*Ti6Al4V*	0.2888	0	1.108×10^{-4}	0	0
	ZrO_2	0.3330	0	0	0	0
κ (W m^{-1} K)	*Ti6Al4V*	6.10	0	0	0	0
	ZrO_2	1.78	0	0	0	0

Table 3
Convergence test of the first four frequencies [Hz] of a simply supported curved beam.

R/L	Approach	Number of elements	f_1	f_2	f_3	f_4
0.5	Analytical		18.6947	118.7263	286.4234	520.8089
	FEM	2	18.6952	118.7714	289.7632	529.4434
		5	18.6949	118.7264	286.4344	520.8664
		10	18.6947	118.7264	286.4303	520.8119
1.0	Analytical		29.7444	130.6730	298.7459	533.6442
	FEM	2	29.7464	130.7138	301.3524	570.9103
		5	29.7445	130.6733	298.7492	533.7051
		10	29.7444	130.6732	298.7464	533.6587
1.5	Analytical		31.9183	132.9281	301.0083	536.0203
	FEM	2	31.9282	132.9684	303.4761	571.6260
		5	31.9184	132.9284	301.0201	536.0772
		10	31.9184	132.9282	301.0170	536.0338

In Table 3 the convergence of the first four frequencies is presented. Notice that with FE models of at least five elements, it is possible to guarantee differences lower than 0.1% in the first four frequencies. In this case the test values are the frequencies calculated with the analytical solution derived in the previous section. The same can be said in the case of buckling problems. In fact, Fig. 2 shows a convergence analysis of the buckling eigenvalue problem of curved beams with clamped ends and load Q_y^0 applied at $x = L/2$, directed toward the curvature center. The curved beam is such that $R = 1.0$ m, with a rectangular cross-section that has radial width $h = 0.05$ m and height $b = 0.01$ m. The material properties vary from a metallic surface (SUS302 at $z = -b/2$) to a ceramic surface (Alumina at $z = b/2$) according to the power law given in Eq. (29) with $n = 1$.

4.2. Comparisons with experimental data: the straight beam case

The curved beam model developed in this paper can be reduced to the case of a straight beam if the condition $R \to \infty$ is imposed. Then, as a first example the values of free vibration frequencies obtained experimentally by Kapuria et al. [26] are compared with the frequencies calculated with the present curved beam model, but reduced to the case of a straight beam. Kapuria et al. [26] tested cantilever beams with three or five layers composed by different mixtures of aluminium and silicon carbide [26]. The material properties are given in Table 1, whereas the mixture ratio Al/SiC can be {100/0, 80/20, 60/40} and {100/0, 90/10, 80/20, 70/30, 60/40} for the configurations of three and five layers, respectively. The thickness of each layer is 3 mm (2 mm) for the configuration of three (five) layers, whereas the width of the beam is 15 mm. The constitutive law to calculate the longitudinal modulus of elasticity is given in Eq. (33), which is a variety of the two-constituents rule of mixtures [27], whereas the variation of the density and Poisson's coefficient can be characterized with the classic linear rule of mixtures given by Eq. (34).

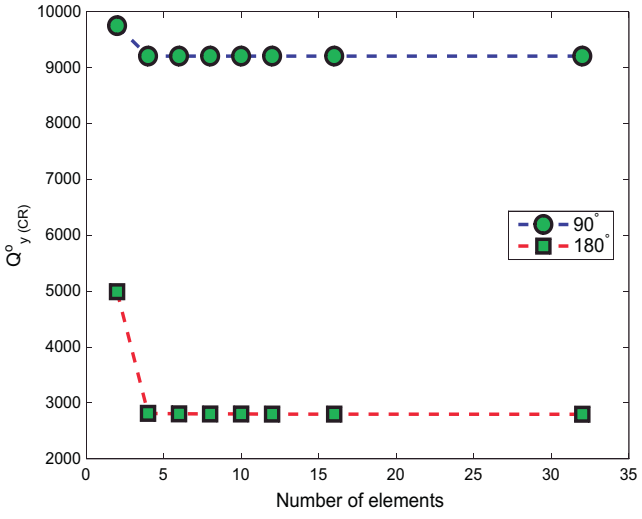

Fig. 2. Convergence of the buckling load for two different cases of subtended angles.

$$E_{xx} = \frac{[V_m E_m (q_\sigma + E_c) + (1 - V_m)(q_\sigma + E_m) E_c]}{[V_m (q_\sigma + E_c) + (1 - V_m)(q_\sigma + E_m)]} \tag{33}$$

$$p_{fgm} = V_m p_m + V_c p_c \tag{34}$$

where V_m and V_c are the volumetric proportions of metallic and ceramic constituents, respectively. E_m and E_c are the longitudinal modulus of elasticity of metallic and ceramic constituents, respectively. p_{fgm}, p_m and p_c identify a generic property of the FGM, the metallic constituent and the ceramic constituent, respectively. $q_\sigma = -(\sigma_c - \sigma_m)/(\varepsilon_c - \varepsilon_m)$ is the ratio of stress to strain transfer between the metallic and ceramic phases. If $q_\sigma = \infty$, which means equal strain transfer, Eq. (33) can be reduced to Eq. (34). The value $q_\sigma = 91.6$ GPa for the material *Al/SiC* was experimentally determined [26].

Table 4 shows the comparison of the first four natural frequencies obtained experimentally [26] and the ones calculated by the finite element approach of the present paper. The experimental data of three samples and their mean value are contrasted with a numerical model of four finite element of five nodes. Also a 3D finite element calculation carried out in the commercial program COSMOS/M (with models of more than 5000 tetrahedral elements of cubic interpolation [32]) is presented to check the results of the 1D models. Table 5 shows the comparison of the first four natural frequencies [26] of samples with five layers. It is possible to see a quite good correlation of the 1D finite element approach with the experimental data available, which are also comparable with the results of the 3D finite element method.

4.3. Comparisons with other approaches

This section describes the comparison of the present model with other curved beam models [14,28]. The curved beam is isotropic with a cross-section having equal height and depth ($b = h$). The Poisson's coefficient is $\mu = 0.3$. The shear stiffness is affected by a shear correction coefficient $k_s = 0.85$ and the geometrical features of the beam are such that $S_r = R/h\sqrt{12} = 100$ [28]. The following non-dimensional frequency parameter is used [28]:

$$\overline{\Omega}_i = \Omega_i R^2 \sqrt{\frac{\mathbf{M}_{m44}}{\mathbf{J}_{22}}}, \quad i = 1, 2, 3. \tag{35}$$

Table 6 shows the non-dimensional natural frequency parameters of a clamped–clamped curved beam. It is possible to see a quite good agreement of the three approaches. In fact differences in percentage not higher than 0.6% can be observed.

Table 6
Comparison of the first three non-dimensional natural frequency parameter.

Opening angle	Approach	$\overline{\Omega}_1$	$\overline{\Omega}_2$	$\overline{\Omega}_3$
60	Malekzadeh [14]	19.398	54.014	105.611
	Tufekci [28]	19.402	54.031	105.651
	Present Model	19.442	54.093	105.707
120	Malekzadeh (2010)	4.452	12.825	25.984
	Tufekci (2006)	4.451	12.826	25.989
	Present Model	4.471	12.885	26.064
180	Malekzadeh (2010)	1.805	5.198	10.918
	Tufekci (2006)	1.804	5.198	10.918
	Present Model	1.817	5.239	10.984

The subsequent studies correspond to the comparison of the present model with a full 3D approach of a curved beam with graded properties. The full 3D calculation is performed with a flexible 3D general solver of partial differential equations (called FlexPDE) within the context of the finite element method. In this solver it possible to easily cope with the complex material laws incorporated in the structural model as well as the model itself (see http://www.pdesolutions.com [29] and the work of Ramirez and Piovan [30] for further explanations). The curved beam has a curvature radius $R = 1$ m and a solid rectangular cross-section with a depth $h = 0.02$ m in the radial direction and a height $b = 0.01$ m. The material properties can vary according to one of the variation laws given in Eq. (29). In both cases the inner material constituent is steel and the outer material is alumina. The shear modulus of elasticity (when properties of the constituents are not provided) can be calculated by means of the common law of elastic proportionality between shear and longitudinal elasticity modulus (i.e. $2G = E/(1 + \nu)$). The structure is discretized with five curved beam elements in the 1D formulation and with no less than 4000 tetrahedral finite elements of cubic approximation in the 3D formulation. Table 7 shows the in-plane frequencies calculated with both approaches employing the first rule of Eq. (29), whereas Table 8 describes the out-of-plane frequencies calculated with both approaches but employing the second rule of Eq. (29). A good agreement between both formulation can be observed for different parametric ratios. Moreover, in these tables differences in percentage no higher than 2–3% can be observed. This implies that the present 1D beam model can be an efficient tool to predict frequencies for thin or even thick curved beams with functionally graded material properties.

Table 9 depicts the first three buckling loads of FG curved beams calculated with the present 1D approach and 3D finite

Table 4
Natural frequencies [Hz] of a cantilever Al/SiC beam with three layers.

Mode no.	Ref. [26]					Present work	
	Exp. No. 1	Exp. No. 2	Exp. No. 3	Exp. mean	Beam model	3D	1D
1	837	890	820	849	840	814	827
2	5265	5410	5015	5230	5075	4925	4996
3	14,100	14,550	13,590	14,080	12,486	13,105	13,273
4	15,005	15,100	15,000	15,035	14,447	14,286	14,234

Table 5
Natural frequencies [Hz] of a cantilever Al/SiC beam with five layers.

Mode no.	Ref. [26]					Present work	
	Exp. No. 1	Exp. No. 2	Exp. No. 3	Exp. mean	Beam model	3D	1D
1	761	726	770	752	754	749	757
2	4592	4387	4670	4550	4558	4523	4572
3	12,318	11,790	12,420	12,176	12,125	12,019	12,136
4	13,464	13,355	13,465	13,428	13,078	12,994	12,900

Table 7
In-plane natural frequencies [Hz] of a cantilever curved beam graded in the radial direction. Comparison with a 3D FEM approach.

n	Mode no.	FEM 3D approach h/L			Present 1D approach h/L		
		0.025	0.050	0.100	0.025	0.050	0.100
0.1	1	52.83	209.10	831.29	52.67	208.34	826.11
	2	304.59	1266.46	4938.81	303.46	1261.63	4907.12
	3	883.62	3512.02	12597.07	879.53	3497.80	12537.10
	4	1741.68	6407.17	13235.34	1730.51	6385.10	13157.10
1	1	40.62	160.77	638.79	40.54	160.32	635.56
	2	233.80	972.22	3777.20	233.49	970.32	3768.56
	3	677.09	2689.84	9263.90	676.56	2687.77	9240.45
	4	1331.02	4704.51	9967.55	1330.45	4699.85	9972.27
10	1	30.0	119.01	472.90	30.01	118.72	470.75
	2	172.70	720.61	2808.79	172.92	718.91	2796.19
	3	500.59	1997.47	6968.74	501.15	1992.85	6948.88
	4	984.60	3539.04	7459.85	985.87	3533.46	7427.33

Table 8
Out-of-plane natural frequencies [Hz] of a cantilever curved beam graded in the z-direction. Comparison with a 3D FEM approach.

n	Mode no.	FEM 3D approach h/L			Present 1D approach h/L		
		0.025	0.050	0.100	0.025	0.050	0.100
0.1	1	25.50	103.71	415.46	25.78	104.63	415.91
	2	147.66	626.44	2554.42	149.13	639.74	2557.76
	3	429.58	1772.98	7069.07	438.03	1797.47	7077.82
	4	829.09	3521.25	13514.06	853.47	3567.15	13457.8
1	1	20.42	80.55	322.31	20.37	80.74	320.19
	2	118.15	492.07	1980.57	117.27	492.62	1969.96
	3	343.46	1383.59	5469.64	341.79	1382.74	5402.62
	4	680.43	2725.98	10401.69	674.63	2673.20	10334.6
10	1	14.82	59.37	237.74	15.04	59.80	237.25
	2	85.68	362.97	1462.73	87.46	366.66	1461.48
	3	248.25	1020.52	4046.95	252.99	1026.53	4015.65
	4	490.99	2012.39	7713.62	499.06	2000.33	7669.83

Table 9
Comparison between the present 1D model and 3D finite element models: buckling load Q_y^0 applied at $x = L/2$ for the clamped–clamped case or $x = L$ for the clamped-free case.

Bound. cond.	Clamped–clamped				Clamped-free			
Arch angle	180°		90°		180°		90°	
Approach	1D	3D	1D	3D	1D	3D	1D	3D
Mode 1	11,223	11,218	38,246	38,600	1353	1340	4426	4417
Mode 2	44,540	44,559	101,670	101,500	7002	6930	17,836	16,989
Mode 3	65,237	64,715	165,950	167,255	13,442	12,980	31,311	30,504

element models. The buckling loads of the 3D formulation are calculated with the commercial software COSMOS/M [32]. For the computation of the buckling loads of the aforementioned table, ten 1D curved finite elements are employed whereas models of more than 2500 hexahedral finite elements are tested in COSMOS/M. The curved beam is completely made of steel (see Table 3). The curved beam has a radius $R = 0.5$ m, and a solid rectangular cross-section of radial width $h = 0.05$ m and height $b = 0.01$ m. The curved beam can be clamped at both ends with a load Q_y^0 applied at $x = L/2$, or it can be clamped-free with a load Q_y^0 applied at the free end. In both cases the force is directed towards the center of curvature. As one can see in Table 8 the present one dimensional curved beam model agrees very well with numerical 3D approaches.

4.4. Instability of curved beams made of FGM: parametric studies

In this section a parametric study related to the variation of the buckling loads with several parameters is presented. Two different types of configurations are selected: a bi-clamped arch with a load Q_y^0 located at $x = L/2$ and directed toward the center of curvature, and a cantilever arch with the same type of load but located at $x = L$. In both cases the cross-section is rectangular with radial width $h = 0.05$ m and a thickness $b = 0.01$ m. The variation of the buckling loads is analyzed with respect to the opening angle of the curved beam. The circumferential length of the curved beam is fixed in the value $L = 1$ m and the buckling load is computed for different curvature radius R.

In Figs. 3 and 4 it is shown the variation of the buckling loads for the cantilever case and bi-clamped case, respectively. In both cases the variation of the buckling load with respect to the subtended angle L/R is shown. The material properties of these two cases are graded from steel to alumina in the y-direction according to the power law given in Eq. (30). Four different cases of power law index n are compared in these figures. If the power law index $n \to 0 (n \to \infty)$ the curved beam is completely constructed with alumina (steel). Note that the case $L/R = 0$ identifies a straight

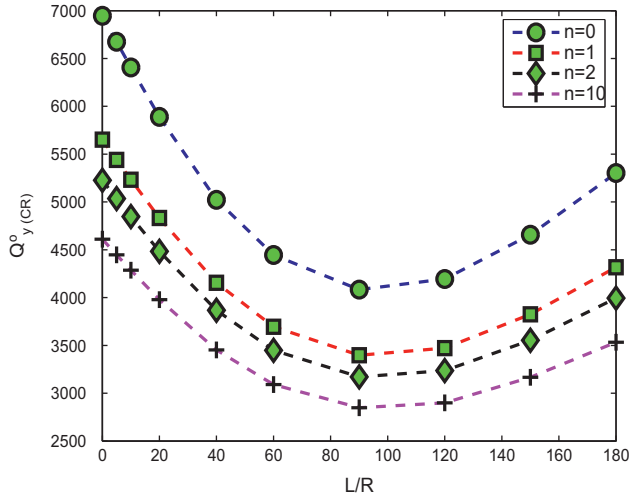

Fig. 3. Variation of the buckling load with the opening angle for a cantilever curved beam.

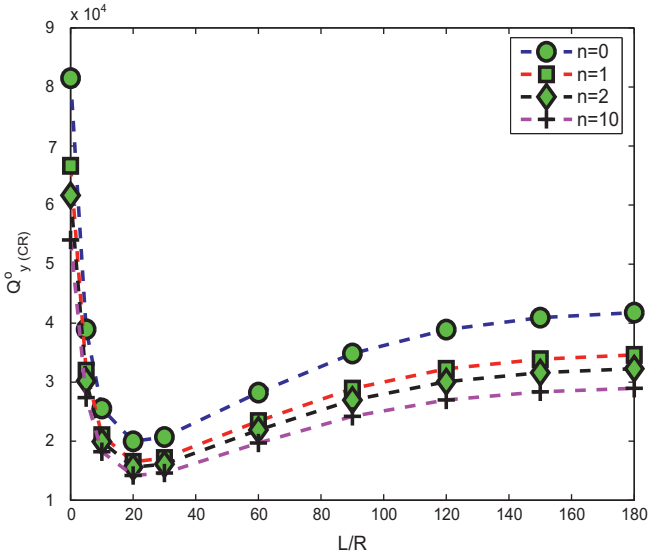

Fig. 4. Variation of the buckling load with the opening angle for a bi-clamped curved beam.

beam. Notice that the buckling load has a minimum value at a certain subtended angle. This subtended angle is related to the boundary conditions, the geometrical properties and the position of the load, however it is not heavily influenced by the value of the power law index n.

Fig. 5 shows the variation of the buckling loads of a cantilever curved beam subjected to three uniform thermal states, $T = 100$ K, $T = 300$ K and $T = 500$ K. The material properties of the beam are summarized in the Table 2. The beam has a solid rectangular cross-section with radial width $h = 0.05$ m and a thickness $b = 0.01$ m, and its length is $L = 1.0$ m. The properties are graded according to the first of Eq. (29) with $n = 2$ and a metallic core ($Ti6Al4V$) surrounded by ceramic surfaces (ZrO_2). The load Q_y^0 is located at $x = L$ and directed towards the center of curvature. Note that as the environment temperature is increased the buckling loads are substantially lower due to a loss of material strength associated to the elastic moduli E_{xx}, G_{xy} and G_{xz}, that it is possible to infer according to Eq. (15). The readers interested in thermal instability of curved beams can follow very recent specific Refs.

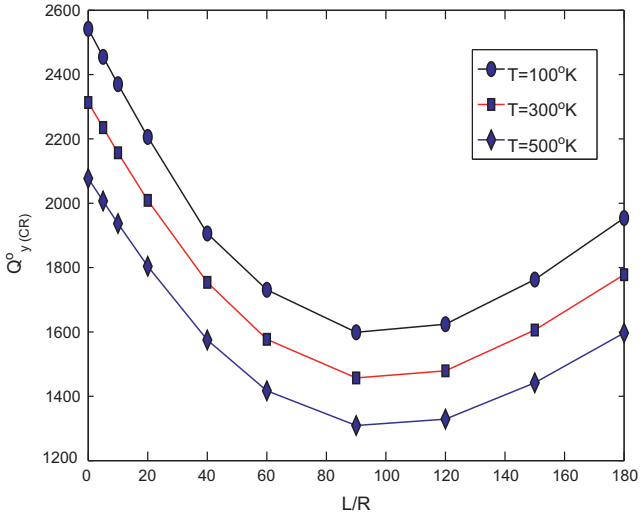

Fig. 5. Variation of the buckling load with respect to the opening angle of a cantilever curved beam for three different temperatures.

[33,34] that are beyond the scope and interests of the present article.

4.5. Dynamics of curved beams made of FGM under the presence of initial stresses

In this section an analysis of the dynamic response of functionally graded curved beams subjected to initial stresses is carried out. The curved beam has material properties that are graded from steel to alumina in the y-direction according to the power law given by Eq. (30). The beam ends can be clamped–clamped or clamped-free. The initial load Q_y^0 is located at $x = L/2$ ($x = L$) in the clamped–clamped (clamped-free) case and directed towards the center of curvature. The beam has a curvature radius $R = 1$ m. Now, in Fig. 6 it is possible to see the variation of the first frequency of the clamped–clamped curved beam with respect to the load coefficient $\lambda = Q_y^0/Q_{y_{ref}}^0$, where $Q_{y_{ref}}^0$ is the buckling load. Two opening angles, 90° and 180° and three graded configurations were tested.

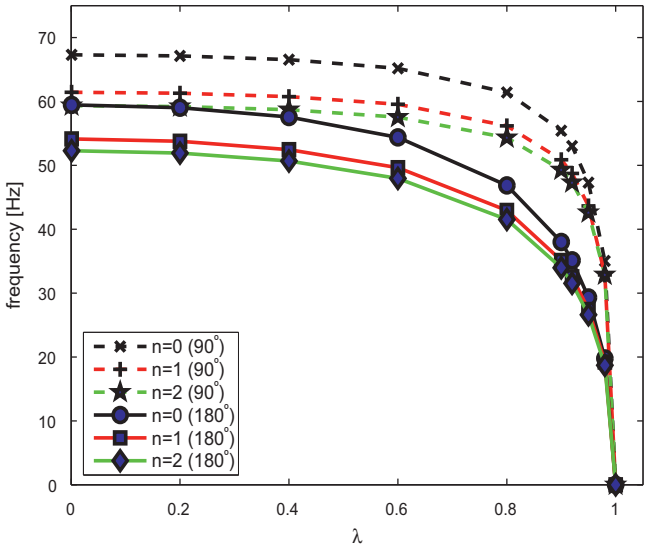

Fig. 6. Variation of the first frequency versus the coefficient $\lambda = Q_y^0/Q_{y_{ref}}^0$ for a clamped–clamped curved beam with Q_y^0 applied at $x = L/2$. $Q_{y_{ref}}^0$ is the buckling load for the corresponding case.

As one can see the frequency values fall from the unloaded case (i.e. $\lambda = 0$) to the buckled state (i.e. $\lambda = 1$), where frequency values are zero. In Fig. 7 it is possible to see the variation of the first frequency of the clamped-free curved beam with respect to the load coefficient $\lambda = Q_y^0/Q_{y_{ref}}^0$, where $Q_{y_{ref}}^0$ is the corresponding buckling load of the present case.

Fig. 8 depicts the variation of the first frequency of a clamped–clamped curved beam with respect to the load coefficient λ related to a tangential initial force Q_x^0. The initial force is located at $x = L/2$ and directed tangentially in positive x-direction. In this case the coefficient λ is defined as $\lambda = Q_x^0/Q_{x_{ref}}^0$, where the reference initial force $Q_{x_{ref}}^0$ corresponds to the buckling load. The opening angle of the curved beam is 180° and the material distribution and geometric dimensions are the same as in the case of the previous two figures.

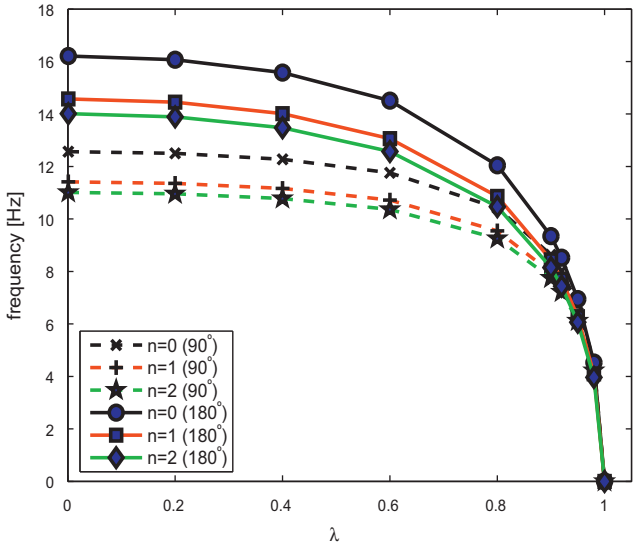

Fig. 7. Variation of the first frequency versus the coefficient $\lambda = Q_y^0/Q_{y_{ref}}^0$ for a clamped-free curved beam with Q_y^0 applied at $x = L$. $Q_{y_{ref}}^0$ is the buckling load for the corresponding case.

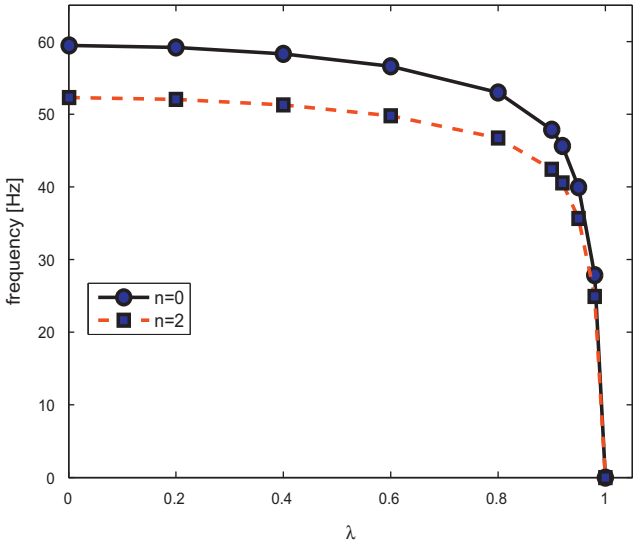

Fig. 8. Variation of the first frequency versus the coefficient $\lambda = Q_x^0/Q_{x_{ref}}^0$ for a clamped–clamped curved beam of $\beta = 180°$ with Q_x^0 applied at $x = L/2$. $Q_{x_{ref}}^0$ is the buckling load.

Table 10
First and second frequencies of arches with initial stresses. Q_{yCr}^0 is the buckling load.

Bound. cond.	Angle	$Q_y^0 = 0$	$Q_y^0 = 1/2Q_{yCr}^0$	$Q_y^0 = 2/3Q_{yCr}^0$
Clamped–clamped	90	61.34 (*OP*)	44.01 (*OP*)	36.13 (*OP*)
		174.59 (*OP*)	157.53 (*OP*)	151.37 (*OP*)
	180	54.34 (*OP*)	39.13 (*OP*)	32.17 (*OP*)
		157.40 (*OP*)	147.62 (*OP*)	144.18 (*OP*)
Clamped-free	90	11.32 (*OP*)	8.31 (*OP*)	6.88 (*OP*)
		54.48 (*IP*)	54.18 (*IP*)	54.08 (*IP*)
	180	14.48 (*OP*)	10.59 (*OP*)	8.75 (*OP*)
		42.17 (*OP*)	41.67 (*OP*)	41.51 (*OP*)

In Table 10 it is possible to see a comparison of the influence of the initial stresses on the frequency values of clamped–clamped and clamped-free FG curved beams for two load intensity conditions. The load Q_y^0, which is parameterized with respect to the corresponding buckling load Q_{yCr}^0, is applied at $x = L/2$ and $x = L$ for the clamped–clamped case and clamped-free case, respectively. In both cases the load is oriented towards the curvature center of the beam. The material properties of the beam are radially distributed, according to Eq. (30), from alumina (at $y = h/2$) to steel (at $y = -h/2$). In the table the acronyms (OP) and (IP) mean "out-of-plane" modes and "in-plane" modes, respectively. Notice that the first frequency is highly influenced by initial stresses whereas the higher modes are slightly influenced by the same load condition. Particularly the out-of-plane modes are more influenced by in-plane initial stresses as one can see in the table.

4.6. Dynamics of graded thin-walled curved beams

This paragraph shows the results of a study on the dynamics of functionally graded thin walled curved beams with open cross-sections. The cross-section of this example is an arc of radius $R_C = 0.05$ m, thickness $b_w = 0.01$ m and opening angle $\alpha = 60°$ (see the detail in Fig. 9). The curved beam has clamped ends and an opening angle $\beta = 180°$. The material properties are graded according to Eq. (32), with an inner core of aluminum and external surfaces of silicon carbide (see Table 1). The symmetry of the material properties with respect to the middle line of the cross-section as well as the cross-sectional symmetry with respect to

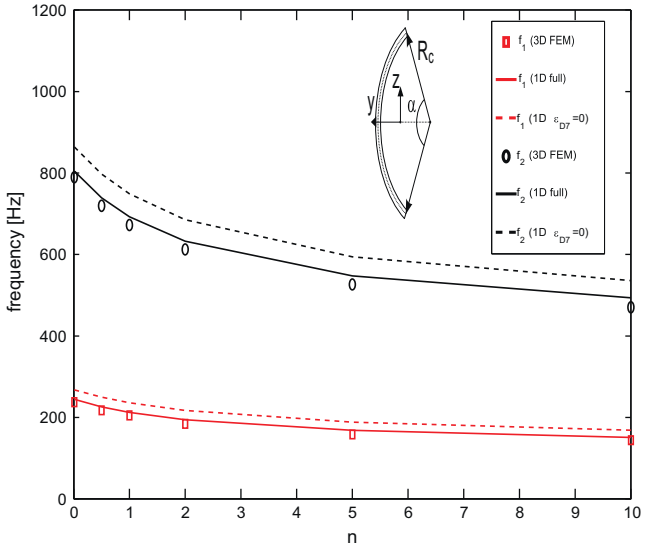

Fig. 9. Variation of the first and second out-of-plane frequencies against the power index n for a thin walled curved beam: comparison of modeling topics with 3D computational approaches.

the curvature plane, allow the decoupling of the motion equations into in-plane and out-of-plane motions. This simplify substantially the analysis of statics and dynamics problems.

The Fig. 9 shows the variation of the first two out-of-plane free vibration frequencies with respect to the power law index n. Two modeling alternatives of the curved beam are compared with respect to a 3D numerical approach [29] that also serves as validation. Models of ten beam element and more than 10,000 tetrahedral elements of cubic interpolation [29] were employed. On one hand, the differences of the frequencies calculated with the full shear deformable curved beam with respect to the ones calculated with the 3D approach oscillate in the range 3–8%, which is an acceptable difference between 1D and 3D approaches (see also the Section 4.3). On the other hand, if the shear deformation due to non-uniform torsion-warping is neglected (i.e. $\varepsilon_{D7} = 0$), the above mentioned differences are in the range 15–22%. As one can see the incorporation of shear flexibility due to non-uniform torsion-warping plays an important role in the case of curved beam with thin walled cross-section. This effect is more important in higher frequencies as it can be concluded from this example and as was shown also in papers about straight and curved beams constructed with composite materials [20,35] or isotropic materials [36].

A last example is presented with the aim to quantify the effect of the proportional damping in the dynamics of FG curved beam. The curved beam has the same boundary conditions, mechanical and geometrical properties of the previous example, i.e. a thin-walled curved beam with an open cross-section. The beam is excited by an impact force $\widetilde{\mathbf{F}} = 100\{\hat{\mathbf{y}}, \hat{\mathbf{z}}\}N$ (with $\hat{\mathbf{y}}$ and $\hat{\mathbf{z}}$ being the unitary vectors), applied at $x = 0.4L$. The damping coefficients are assumed with the same value (i.e. $\xi_1 = \xi_2 = \xi$) just for comparison purposes. The velocity of the system can be calculated, in the frequency domain, appealing to [25] $\mathbf{V}(\Omega) = i\Omega[\mathbf{H}(\Omega)]^{-1}\mathbf{F}(\Omega)$, where $\mathbf{F}(\Omega)$ is the excitation force in the frequency domain, $\mathbf{H}(\Omega) = -\Omega^2\mathbf{M} + i\Omega\mathbf{C}_{RD} + \mathbf{K}$ and Ω is the circular frequency.

The Fig. 10 shows the variation of velocity amplitude $|\dot{u}_{yc}(L/2)|$ corresponding to the first and second in-plane modes with respect to the damping coefficient. Three functionally graded distributions are involved, i.e. with power law indexes $n = 0.1$, $n = 1.0$ and $n = 10$ in Eq. (32). These indexes can cover a range of materials from a configuration richer in ceramic phase ($n = 0.1$) to a configuration richer in metallic phase ($n = 10$). Notice that when the material configuration is richer in ceramic phase, the response is more damped. This is a direct consequence of the stiffness (E) and mass (ρ) properties of the ceramic constituent that are higher than the metallic counterpart.

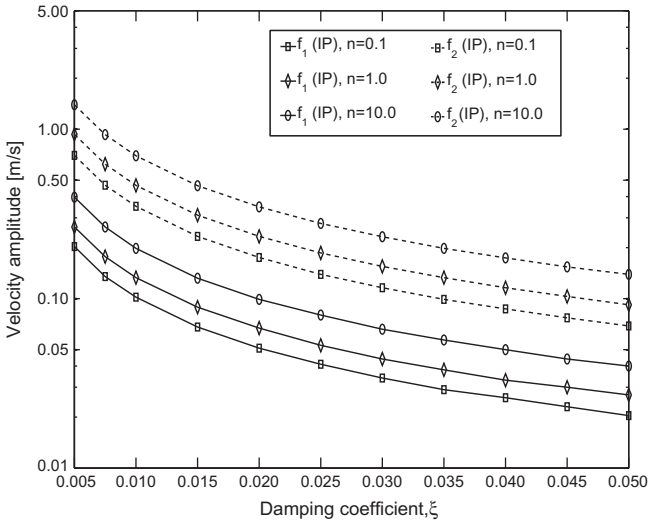

Fig. 10. Variation of the velocity amplitude $|\dot{u}_{yc}(L/2)|$ of the first two in-plane frequencies with respect to the damping coefficient ξ.

5. Conclusions

In this paper, a general model for curved beams constructed with functionally graded materials has been introduced. The model has been deduced applying the linearized principle of virtual work based on a displacement field with first- and second-order terms. Shear flexibility due to bending and non-uniform warping has been taken into account. Arbitrary states of initial stresses and initial volume and surface forces, general initial off-axis forces have been incorporated. The present model can be employed for dealing with general linearized dynamic and stability problems as well as general static problems of functionally graded curved beams. The model can be decoupled into in-plane and out-of-plane motions if appropriate restrictions in the geometry and the gradation of material properties are used. The importance of different modeling aspects, such as shear deformation due to non-uniform torsion-warping, damping and initial stresses among others has been analyzed and appropriately characterized. Moreover, the curved beam model can be reduced to a straight beam model and it is quite efficient, predicting very well experimental results as well as results of full 3D finite element approaches. This point is very important if time cost is crucial, especially in active control, structural optimization and dynamics with uncertain parameters which are the topics of subsequent investigation.

Acknowledgement

The support of Universidad Tecnológica Nacional and CONICET is recognized.

Appendix A. Calculation of the warping function of a straight bar

The function $\bar{\omega}(y,z)$ is case dependent of the material gradation distribution in the cross-section (i.e. the variation of the elastic material properties) and it can be calculated by solving the following differential equations [23]:

$$\begin{aligned} &\frac{\partial}{\partial z}\left(\frac{1}{G_{xy}}\frac{\partial \psi}{\partial z}\right) + \frac{\partial}{\partial y}\left(\frac{1}{G_{xz}}\frac{\partial \psi}{\partial y}\right) = -2\Theta, \\ &\frac{\partial}{\partial z}\left(G_{xz}\frac{\partial \bar{\omega}}{\partial z}\right) + \frac{\partial}{\partial y}\left(G_{xy}\frac{\partial \bar{\omega}}{\partial y}\right) - \Theta\left(z\frac{\partial G_{xy}}{\partial y} - y\frac{\partial G_{xz}}{\partial z}\right) = 0, \end{aligned} \tag{A.1}$$

where, $G_{xy} \equiv G_{xy}(y,z)$ and $G_{xz} \equiv G_{xz}(y,z)$ are the shear moduli that can vary according to a given rule; Θ is a prescribed twisting angle per unit length employed to normalize the warping function and ψ is the so called Prandtl stress-function employed to define the shear stresses σ_{xy} and σ_{xz} in terms of spatial derivatives. These equations are subjected to the following boundary conditions:

$$\begin{aligned} &\psi = 0, \text{on } \Lambda_0, \\ &\frac{\partial \bar{\omega}}{\partial n} = \left\{\frac{\partial \psi}{\partial z} + \Theta G_{xy} z, -\frac{\partial \psi}{\partial y} - \Theta G_{xz} y\right\} \times \hat{n}_u, \text{ on } \Lambda_0. \end{aligned} \tag{A.2}$$

In previous equation, Λ_0 is the contour of the cross-section, $\hat{n}_u$ is the unit vector normal to the cross-sectional contour and $\partial(\bullet)/\partial n$ is the normal derivative operator and $\times$ is the internal product operator.

Normally if the shear moduli are graded according to an arbitrary distribution, $\bar{\omega}$ has to be calculated with computational approaches [30]; however under certain conditions and type of gradation law, $\bar{\omega}$ may be calculated with a closed form solution in the form suggested by Lekhnitskii [23].

Appendix B. Extended definition of matrices and vectors employed in the principle of virtual works

In this Appendix the expressions introduced in paragraph 2.2 are properly characterized for the sake of clarity. Then, the matrix of all initial stress resultants $\mathbf{T}^0$ is defined as follows:

$$\mathbf{T}^0 = \begin{bmatrix} \mathbf{T}^0_{11} & 0 & \mathbf{T}^0_{13} & 0 \\ 0 & \mathbf{T}^0_{22} & \mathbf{T}^0_{23} & 0 \\ \mathbf{T}^0_{31} & \mathbf{T}^0_{32} & \mathbf{T}^0_{33} & \mathbf{T}^0_{34} \\ 0 & 0 & \mathbf{T}^0_{43} & 0 \end{bmatrix} \tag{B.1}$$

where

$$\mathbf{T}^0_{11} = \int_A \sigma^0_{xx} \tilde{\mathbf{g}}^T_a \tilde{\mathbf{g}}_a \mathcal{F}\, dy\, dz, \quad \tilde{\mathbf{g}}_a = \{1, z, -y, -\omega\} \tag{B.2}$$

$$\mathbf{T}^0_{22} = \int_A \sigma^0_{xx} (\tilde{\mathbf{g}}^T_b \tilde{\mathbf{g}}_b + \tilde{\mathbf{g}}^T_c \tilde{\mathbf{g}}_c) \mathcal{F}\, dy\, dz, \quad \begin{cases} \tilde{\mathbf{g}}_b = \{1, 0, 0, y\} \\ \tilde{\mathbf{g}}_c = \{0, 1, 0, -z\} \end{cases} \tag{B.3}$$

$$\mathbf{T}^0_{13} = \left(\mathbf{T}^0_{31}\right)^T = \int_A \begin{bmatrix} 0 & \sigma^0_{xz} & -\sigma^0_{xz} & g^0_w \\ 0 & 0 & 0 & g^0_w z \\ 0 & 0 & 0 & -g^0_w y \\ 0 & 0 & 0 & -g^0_w \omega \end{bmatrix} dy\, dz,$$

$$g^0_w = \sigma^0_{xy} \frac{\partial \omega}{\partial y} + \sigma^0_{xz} \frac{\partial \omega}{\partial z} \tag{B.4}$$

$$\mathbf{T}^0_{23} = \left(\mathbf{T}^0_{32}\right)^T = \int_A \begin{bmatrix} -\sigma^0_{xz} & -\sigma^0_{xx} & 0 & 0 \\ \sigma^0_{xy} & 0 & 0 & \sigma^0_{xx}\omega/(R+y) \\ 0 & 0 & 0 & 0 \\ 0 & -\sigma^0_{xx} y & 0 & -\sigma^0_{xx} z\omega/(R+y) \end{bmatrix} dy\, dz, \tag{B.5}$$

$$\mathbf{T}^0_{33} = \int_A \begin{bmatrix} -\sigma^0_{xx} y/R & & & sym \\ \sigma^0_{xy}/2 & \sigma^0_{xx}/\mathcal{F} & & \\ g^0_x/R - \sigma^0_{xz}/2 & \sigma^0_{xx} z/2R & \sigma^0_{xx} & \\ \sigma^0_{xx}\omega/R & 0 & \sigma^0_{xx}\omega/R & \sigma^0_{xx}\omega^2/(R+y) \end{bmatrix} dy\, dz \tag{B.6}$$

$$\mathbf{T}^0_{34} = \left(\mathbf{T}^0_{43}\right)^T = \int_A \begin{bmatrix} 0 & \sigma^0_{xx} y/2 & \sigma^0_{xx} z/2 & 0 \\ \sigma^0_{xx} y/2 & 0 & g^0_x/2 & -\sigma^0_{xz}\omega \\ \sigma^0_{xx} z/2 & g^0_x/2 & 0 & \sigma^0_{xy}\omega \\ 0 & 0 & 0 & 0 \end{bmatrix} dy\, dz,$$

$$g^0_x = \frac{\sigma^0_{xy} z - \sigma^0_{xz} y}{2} \tag{B.7}$$

The matrix of initial forces of volume $\mathbf{C}^0_X$ is calculated in the following form:

$$\mathbf{C}^0_X = \frac{1}{2} \int_A \mathbf{T}^T_U \begin{bmatrix} -2\left(\overline{X}^0_y y + \overline{X}^0_z z\right) & \overline{X}^0_x y & \overline{X}^0_x y \\ & -2\overline{X}^0_z z & \overline{X}^0_y z + \overline{X}^0_z y \\ sym & & -2\overline{X}^0_y y \end{bmatrix} \mathbf{T}_U \frac{dy\, dz}{\mathcal{F}} \tag{B.8}$$

where

$$\mathbf{T}_U = \begin{bmatrix} 0 & 0 & 0 & 0 & 0 & 1 & 0 \\ 0 & 0 & 0 & 0 & 1 & 0 & 0 \\ -1/R & 0 & 1 & 0 & 0 & 0 & 0 \end{bmatrix} \tag{B.9}$$

Notice that the matrix of initial forces of surface $\mathbf{C}^0_S$ can be calculated by substituting $\overline{X}^0_i$ for $\overline{S}^0_i$ in the previous expression. On the other hand the matrix $\mathbf{C}^0_X$ can be reconfigured to take into account an off-axis force. This may be done by means of Dirac delta functions, i.e. the initial force of volume $\overline{\mathbf{X}}^0 = \left\{\overline{X}^0_x, \overline{X}^0_y, \overline{X}^0_z\right\}$ is substituted by $\overline{\mathbf{X}}^0 = \delta_B(x_B, y_B, z_B)\overline{\mathbf{F}}^0_B$, where $\overline{\mathbf{F}}^0_B = \left\{\overline{F}^0_{Bx}, \overline{F}^0_{By}, \overline{F}^0_{Bz}\right\}$ is the off-axis force and $\delta_B(x_B, y_B, z_B)$ is the Dirac delta function that identifies the point where the off-axis force is located [20,21].

The vector of external forces $\widetilde{\mathbf{P}}_X$ and the matrix of mass coefficients $\mathbf{M}_m$ can be calculated in the following form:

$$\widetilde{\mathbf{P}}_X = \int_A \begin{bmatrix} \overline{X}_x & \overline{X}_y & \overline{X}_z \end{bmatrix} \mathbf{G}_m \frac{dy\, dz}{\mathcal{F}} \tag{B.10}$$

$$\mathbf{M}_m = \int_A \rho(y, z) \mathbf{G}^T_m \mathbf{G}_m \frac{dy\, dz}{\mathcal{F}} \tag{B.11}$$

where

$$\mathbf{G}_m = \begin{bmatrix} 1 + y/R & 0 & -y & 0 & z - \omega/R & 0 & -\omega \\ 0 & 1 & 0 & 0 & 0 & -z & 0 \\ 0 & 0 & 0 & 1 & 0 & y & 0 \end{bmatrix} \tag{B.12}$$

References

[1] Reddy JN. Analysis of functionally graded plates. Int J Numer Methods Eng 2000;47:663–84.
[2] Reddy JN, Chin C. Thermomechanical analysis of functionally graded cylinders and plates. J Therm Stress 1998;26:593–626.
[3] Praveen G, Chin C, Reddy JN. Thermoelastic analysis of functionally graded ceramic-metal cylinder. J Eng Mech 1999;125:1259–67.
[4] Kitipornchai S, Yang J, Liew K. Semi-analytical solution for nonlinear vibration of laminated fgm plates with geometric imperfections. Int J Solids Struct 2004;41:2235–57.
[5] Hosseini Kordkheili S, Naghdabadi R. Thermoelastic analysis of a functionally graded rotating disk. Compos Struct 2007;79:508–16.
[6] Cheng ZQ, Batra RC. Three dimensional thermoelastic deformations of a functionally graded elliptic plate. Composites: Part B 2000;31:97–106.
[7] Chakraborty A, Gopalakrishnan S, Reddy JN. A new beam finite element for the analysis of functionally graded materials. Int J Mech Sci 2003;45:519–39.
[8] Goupee A, Vel S. Optimization of natural frequencies of bidirectional functionally graded beams. Struct Multidisc Optim 2006;32:473–84.
[9] Ding H, Huang D, Chen W. Elasticity solutions for plane anisotropic functionally graded beams. Int J Solids Struct 2007;44:176–96.
[10] Lü C, Chen W, Xu R, Lim C. Semi-analytical elasticity solutions for bi-directional functionally graded beams. Int J Solids Struct 2008;45:258–75.
[11] Batra RC. Torsion of a functionally graded cylinder. AIAA J 2006;44:1363–5.
[12] Dryden J. Bending of inhomogeneous curved bars. Int J Solids Struct 2007;44:4158–66.
[13] Malekzadeh P. Two-dimensional in-plane free vibrations of functionally graded circular arches with temperature-dependent properties. Compos Struct 2009;91:38–47.
[14] Malekzadeh P, Golbahar Haghighi MR, Atashi MM. Out-of-plane free vibration of functionally graded circular curved beams in thermal environment. Compos Struct 2010;92:541–52.
[15] Piovan MT, Filipich CP, Ramirez JM. A model for shear deformable curved beam made of functionally graded materials. Mecánica Computacional 2008;27:2053–67.
[16] Yousefi A, Rastgoo A. Free vibration of functionally graded spatial curved beams. Compos Struct 2011;93:3048–56.
[17] Filipich CP, Piovan MT. The dynamics of thick curved beams constructed with functionally graded materials. Mech Res Commun 2010;37:565–70.
[18] Shafiee H, Naei M, Eslami M. In-plane and out-of-plane buckling of arches made of fgm. Int J Mech Sci 2006;48:907–15.
[19] Washizu K. Variational methods in elasticity and plasticity. New York, USA: Pergamon Press; 1968.
[20] Piovan MT, Cortínez VH. Mechanics of thin-walled curved beams made of composite materials, allowing for shear deformability. Thin-Wall Struct 2007;45:759–89.
[21] Kim MY, Kim S, Kim N. Spatial stability of shear deformable curved beams with nonsymmetric thin walled sections. I: stability formulation and closed form solutions. Comput Struct 2005;83:2525–41.
[22] Yang Y, Kuo S. Effects of curvature on stability of curved beams. J Struct Eng (ASCE) 1987;113:1185–202.
[23] Lekhnitskii S. Theory of elasticity of an anisotropic body. Moscow, Russia: Mir Publishers; 1982.
[24] Bathe K-J. Finite element procedures in engineering analysis. Englewood Cliffs, New Jersey, USA: Prentice-Hall; 1982.
[25] Meirovith L. Principles and techniques of vibrations. Upper Saddle River, New Jersey, USA: Prentice Hall; 1997.

[26] Kapuria S, Bhattacharyya M, Kumar A. Bending and free vibration response of layered functionally graded beams: a theoretical model and its experimental validation. Compos Struct 2008;82:390–402.
[27] Finot M, Suresh S, Bull C, Sampath S. Curvature changes during thermal cycling of a compositionally graded Ni/Al2O3 multilayered material. Mater Sci Eng A 1996;205:59–71.
[28] Tufekci E, Yasar Dogruer O. Out-of-plane free vibration of a circular arch with uniform cross-section: exact solution. J Sound Vib 2006;291:525–38.
[29] Backstrom G. Deformation and vibration by finite element analysis. Student literatur, Sweden; 1998.
[30] Ramirez JM, Piovan MT. Mechanics of beams with graded properties: comparison of several one-dimensional formulations and higher order formulations based on displacements (In Spanish: Mecánica de vigas con propiedades gradativas: comparación de diversas formulaciones unidimensionales, formulaciones basadas en desplazamientos y de órdenes superiores). Mecánica Computacional 2009;28:729–46.
[31] Argyris JH. An excursion into large rotations. Comput Methods Appl Mech Eng 1982;32:85–155.
[32] COSMOS/M V1.75. User's manual. Structural Research Analysis Corporation, USA; 1997.
[33] Rastgo A, Shafie H, Allahverdizadeh A. Instability of curved beams made of functionally graded material under thermal loading. Int J Mech Mater Des 2005;2(1–2):117–28.
[34] Song X, Li S. Nonlinear stability of fixed-fixed FGM arches subjected to mechanical and thermal loads. Adv Mater Res 2008;33–37:699–706.
[35] Cortínez VH, Piovan MT. Vibration and buckling of composite thin walled beams with shear deformability. J Sound Vib 2002;258(4):701–23.
[36] Cortínez VH, Rossi RE. Dynamics of shear deformable thin walled open beams subjected to initial stresses (in Spanish: Dinámica de vigas con secciones abiertas de paredes delgadas deformables por corte sujetas a un estado inicial de tensiones). Revista Internacional de Métodos Númericos y Cálculo para Ingenería 1998;14(3):293–316.